Mon. Not. R. Astron. Soc. **000**, 1–10 (????) Printed 22 December 2001 (MN LATEX style file v1.4)

On the Formation of Cluster Radio Relics

T. A. Enßlin[1], M. Brüggen[1,2]
[1] *Max-Planck-Institut für Astrophysik, Garching D-85741, Germany*
[2] *Institute of Astronomy, Madingley Road, Cambridge CB3 0HA, United Kingdom*

Accepted ???? Month ??. Received ???? Month ??; in original form ???? Month ??

arXiv:astro-ph/0104233 v2 11 Dec 2001

ABSTRACT

In several merging clusters of galaxies so-called *cluster radio relics* have been observed. These are extended radio sources which do not seem to be associated with any radio galaxies. Two competing physical mechanisms to accelerate the radio emitting electrons have been proposed: (i) diffusive shock acceleration and (ii) adiabatic compression of fossil radio plasma by merger shock waves. Here the second scenario is investigated. We present detailed 3-dimensional magneto-hydrodynamical simulations of the passage of a radio plasma cocoon filled with turbulent magnetic fields through a shock wave. Taking into account synchrotron, inverse Compton and adiabatic energy losses and gains we evolved the relativistic electron population to produce synthetic polarisation radio maps. On contact with the shock wave the radio cocoons are first compressed and finally torn into filamentary structures, as is observed in several cluster radio relics. In the synthetic radio maps the electric polarisation vectors are mostly perpendicular to the filamentary radio structures. If the magnetic field inside the cocoon is not too strong, the initially spherical radio cocoon is transformed into a torus after the passage of the shock wave. Very recent, high-resolution radio maps of cluster radio relics seem to exhibit such toroidal geometries in some cases. This supports the hypothesis that cluster radio relics are fossil radio cocoons that have been revived by a shock wave. For a late-stage relic the ratio of its global diameter to the filament diameter should correlate with the shock strength. Finally, we argue that the total radio polarisation of radio relic should be well correlated with the 3-dimensional orientation of the shock wave that produced the relic.

Key words: galaxies: clusters: general – intergalactic medium – shock waves – magnetohydrodynamics – radio continuum: general – polarization

1 INTRODUCTION

In the current picture of hierarchical structure formation clusters of galaxies grow mainly by the merging of smaller and moderately sized sub-clusters. During such merger events a significant fraction of the kinetic energy of the inter galactic medium (IGM) is dissipated in Mpc-sized shock waves. The shock waves are responsible for heating the IGM to temperatures of several keV. Moreover, they are likely to inject and accelerate relativistic particle populations on cluster scales.

Cluster-wide relativistic electron populations are indeed observed in several merging or post-merging clusters. These electrons reveal their presence by emitting synchrotron emission in the magnetic fields of the IGM to form the so-called *cluster radio halos*. Cluster radio halos have steep radio spectra (spectral index $\alpha \approx 1 - 1.5$); they are unpolarised, and their diffuse morphologies are often similar to those of the thermal X-ray emission of the cluster gas (Govoni et al. 2001). A comparison of the typical radiative lifetime of the radio emitting electrons, which is of the order of 0.1 Gyr, to the typical dynamical timescale of the cluster merger, which is of the order of 1 Gyr, shows that the electron population of a halo cannot be produced directly by a merger shock. Either these electrons have been re-accelerated more recently, or they have been injected by a long-lived shock-accelerated proton population via the hadronic charged pion production. For reviews on recent observations of diffuse cluster radio sources see Feretti (1999), Giovannini, Tordi, Feretti (1999), and Kempner & Sarazin (2001) .

Unlike the radio halos, the so-called *cluster radio relics*[⋆]

[⋆] The name *'cluster radio relic'* was originally chosen in order to reflect the similarities of these sources with *'relic radio galaxies'*. The latter are dying radio cocoons that are no longer supplied with fresh radio plasma from the central parent galaxy. In cluster relics, usually no parent galaxy can be identified. Moreover, they have only been found in clusters of galaxies, and therefore they were named *'cluster radio relics'*. Recently, the connection between cluster radio relics and radio galaxies has been debated.

© ???? RAS

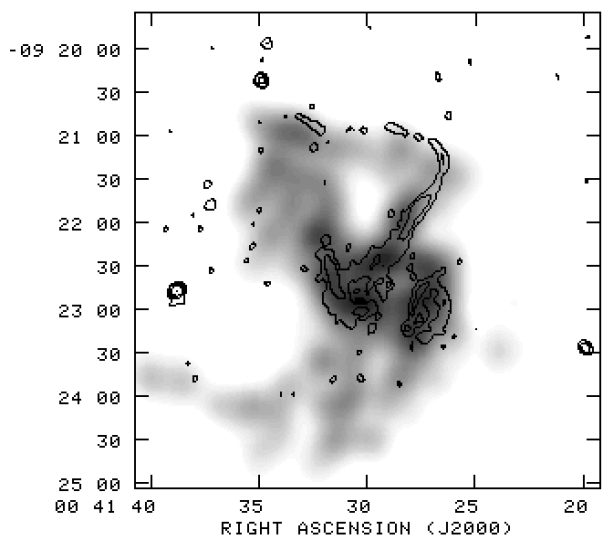

Figure 1. Cluster radio relic in Abell 85 at 327 MHz (grey-scale, Giovannini & Feretti 2000) and at 1.4 GHz (contours, Slee et al. 2001). The 327 MHz maps demonstrates that the thin 1.4 GHz filament extending Northwards belongs in fact to a closed loop in projection. The two smaller, southern blobs on the 1.4 GHz map have also torus-like morphologies.

are more directly related to cluster mergers (Enßlin et al. 1998, Roettiger et al. 1999, Venturi et al. 1999, Enßlin & Gopal-Krishna 2001). They are also extended radio sources with a steep spectrum. In the literature radio relics are often confused with radio halos even though several distinctive properties exist. Cluster radio relics are typically located near the periphery of the cluster; they often exhibit sharp emission edges and many of them show strong radio polarisation.

In several cases it could be shown that shock waves are present at the locations of the relics. In Abell 2256 and Abell 1367 temperature substructures of the hot IGM could be detected (Briel & Henry 1994, Donnelly et al. 1998) which points towards the presence of shock waves at the location of the cluster relics in these clusters. For Abell 754 (Roettiger at al. 1998; Kassim et al. 2001), Abell 2256 (Roettiger et al. 1995), Abell 3667 (Roettiger et al. 1999) and also the Coma cluster (Burns et al. 1994) numerical simulations of mergers were fitted to the X-ray data. These simulations predict shock waves at locations of observed cluster radio relics.

The cluster radio relic 1253+275 in the Coma cluster shows a morphological connection to the nearby radio galaxy NGC 4789 (Giovannini, Feretti & Stanghellini 1991). This suggests that radio relics may be fossil radio plasma that has been revived by a shock. Fossil radio plasma is the former outflow of a radio galaxy in which the high-energy radio emitting electrons have lost their energy. Due to their invisibility in the radio these cocoons are also called *radio ghosts* (Enßlin 1999).

The first relic formation models considered diffusive shock acceleration (Fermi I) as the process producing the radio emitting electrons (Enßlin et al. 1998, Roettiger et al. 1999, Venturi et al. 1999). However, when a fossil radio cocoon is passed by a cluster merger shock wave, with a typical velocity of a few 1000 km/s, the cocoon is compressed adiabatically and not shocked because of the much higher sound speed within it. Therefore, shock acceleration cannot be the mechanism that re-energises the relativistic electron population. But the energy gained during the adiabatic compression combined with the increase in the magnetic fields strength can cause the fossil radio cocoon to emit radio waves again. One prerequisite for this is that the electron population is not older than 0.2 - 2 Gyr (Enßlin & Gopal-Krishna 2001). The timescale depends on the conditions in the surroundings, mainly the external pressure. In high-pressure environments, such as in cluster cores, the synchrotron losses are expected to be much higher due to the higher internal magnetic fields of pressure-confined radio plasma. This leads to a shorter maximum age for the fossil radio plasma if it is to be revived. Therefore, relics are found preferentially at the periphery of clusters where the pressure is lower. Moreover, numerical simulations show that merger shocks are found more frequently in peripheral cluster regions than in the denser cores (Quilis, Ibanez, & Saez 1998; Miniati et al. 2000). Both effects, the longer time for radio plasma to be revivable, and the higher frequency of shock waves could explain why cluster radio relics are more frequently observed at the outskirts of clusters than in more central regions.

Enßlin & Gopal-Krishna (2001) showed that the spectral properties of cluster radio relics are well reproduced by this scenario. Here, we demonstrate that the observed morphologies and polarisation patterns are reproduced by this model as well. This is done with the help of the first 3-dimensional magneto-hydrodynamical (MHD) simulations of a fossil radio cocoon that is passed by a shock wave. We produce artifical radio maps that can be compared directly to high-resolution radio maps of relics.

2 METHOD

2.1 3D MHD Simulation

The magneto-hydrodynamical simulations were obtained using the ZEUS-3D code which was developed especially for problems in astrophysical hydrodynamics (Stone & Norman 1992a, b). The code uses finite differencing on a Eulerian grid and is fully explicit in time. It is based on an operator-split scheme with piecewise linear functions for the fundamental variables. The fluid is advected through a mesh using the upwind, monotonic interpolation scheme of van Leer. The magnetic field is evolved using a modified constrained transport technique which ensures that the field remains divergence-free to machine precision. The electromotive forces are computed via upwind differencing along Alfvén characteristics. For a detailed description of the algorithms and their numerical implementation see Stone & Norman (1992a, b).

Alternative, possibly less misleading names have been proposed, e.g. *'radio flotsam'* by R. Ekers. Here, we use the original terminology a) in order to be consistent with the former literature and b) since our work provides support for a scenario, in which these objects consist of re-illuminated fossil radio plasma, so that they are indeed shock processed relic radio galaxies.

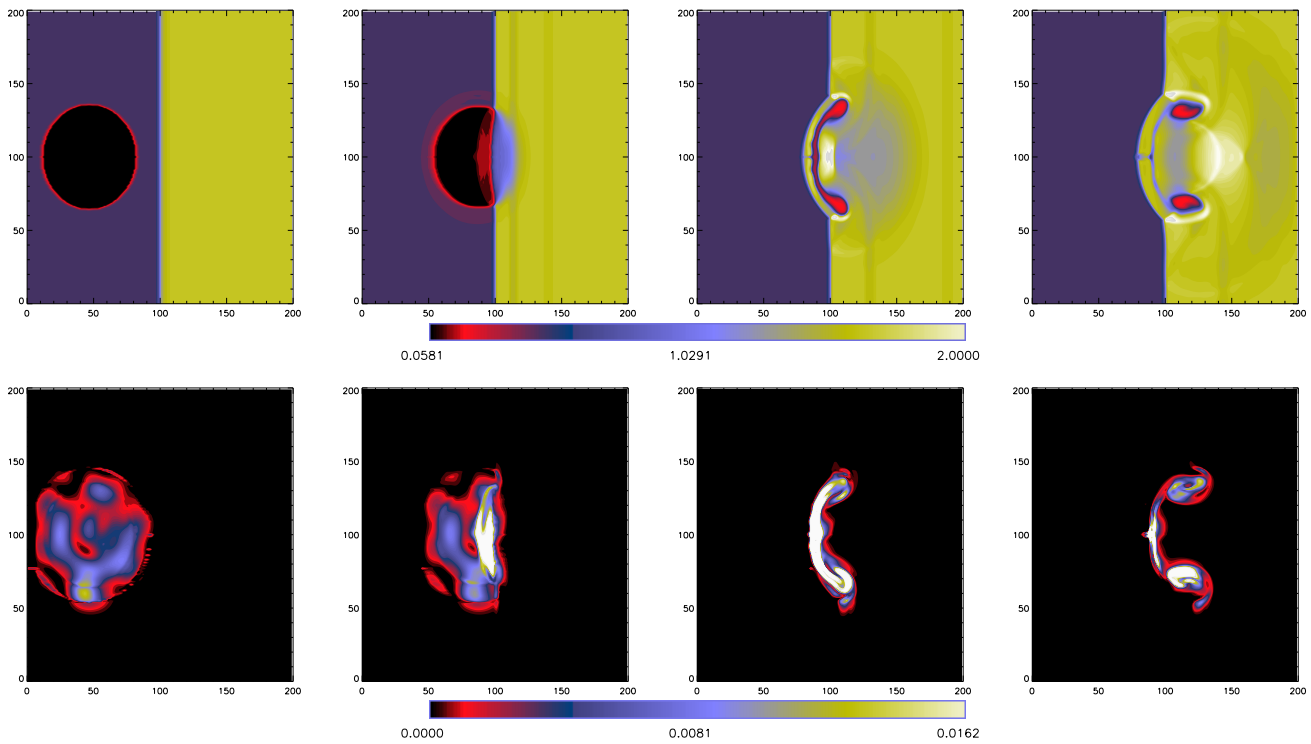

Figure 2. Evolution (from the initial configuration (left) to the final one (right)) of the gas density (top) and magnetic field energy density (bottom) in a central slice through the simulation volume. The pre-shock region is on the left hand side, and the post-shock region on the right hand side of the stationary shock wave, which is located at the centre of the computational box. The formation of a torus is best visible in the density plot. In this simulation the projection of the vector potential of the magnetic fields is not done by Eq. 1, but by the modified form $\mathbf{A} = [\mathbf{I} - g(r)(\mathbf{I} - \hat{\mathbf{r}}\hat{\mathbf{r}})]/(1 - 2\,g(r)/3) \cdot \check{\mathbf{A}}$ in order to have a more uniform magnetic field within the radio cocoon. The numbers on the axes label the zones of the grid.

The simulations were computed on a Cartesian grid with 100^3 and 200^3 equally spaced zones. The fluid flows in the x-direction with inflow boundary conditions at the lower boundary and outflow conditions at the outer boundary. The boundary conditions in the y- and z-directions were chosen to be reflecting. The simulation was set up such that a stationary shock formed at the centre of the simulation box that is perpendicular to the direction of the flow.

In the pre-shock region a spherical bubble of radius R was set up, in which the density was lowered by a factor of 10 with respect to the environment. In turn, the temperature in the bubble was raised such that the bubble remained in pressure equilibrium with its surroundings. Inside the bubble a magnetic field was set up as follows: The magnetic vector potential $\check{\mathbf{A}}$ was composed of 125 Fourier modes with random phases and amplitudes. $\check{\mathbf{A}}$ was then scaled as k^{-3}, where k is the wavenumber of the mode. This leads to a magnetic power spectrum of $P_B(k)\,dk \sim k^{-1}\,dk$. To avoid leakage of the magnetic field into the surroundings of the bubble, we employed the projection:

$$\mathbf{A} = [\mathbf{I} - g(r)(\mathbf{I} - \hat{\mathbf{r}}\hat{\mathbf{r}})] \cdot \check{\mathbf{A}}, \qquad (1)$$

where $\mathbf{I}$ is the identity, r the radius measured from the centre of the bubble, $\hat{\mathbf{r}}$ the corresponding unit vector and $g(r) = (r/R)^2$ if $r < R$ and $g(r) = 1$ if $r \geq R$.

The bubble was filled with around 10^4 uniformly distributed tracer particles that are advected with the flow. We employed a polytropic equation of state with an adiabatic index of $\gamma = 5/3$. The simulations with the serial version of the code were performed on a SUN ULTRA 10 workstation and the parallel version of the code was run on 8 processors on an SGI ORIGIN 3000.

Finally, we should address some issues related to the accuracy of these kinds of finite-difference hydrodynamical simulations. First, one can note that the gas density in the bubble increases with time. Any observed diffusion is entirely numerical. The boundary between the bubble and the ambient medium also becomes less sharp as the simulation proceeds due to discretisation errors in the advection scheme. For a test of the advection algorithm in the ZEUS code see Stone & Norman (1992a,b). Simple tests showed that during the advection of a sharp discontinuity over a grid of 200 zones the discontinuity is spread over 3-4 grid cells. Therefore, the smaller features in our simulation are more susceptible to advection errors than the larger ones.

Second, numerical viscosity is responsible for suppressing small-scale instabilities at the interface between the bubble and the cooler, surrounding gas. To assess the effects of numerical viscosity, we have repeated our simulations in 2D on grids with 300^2 and 500^2 grid points. Finally, we found that numerical resistivity destroys the magnetic field upon compression by the shock. With the affordable numerical resolution the magnetic field orientation reversals are pressed in very nearby computational cells. This is discussed further in Sec. 3.2.

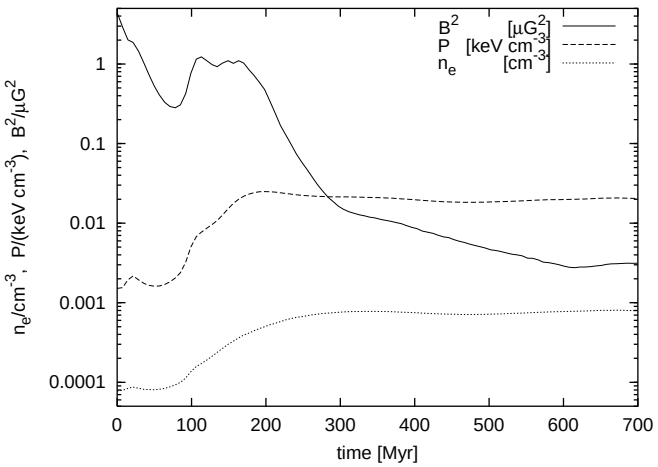

Figure 3. Evolution of the average magnetic field energy density $\sim B^2$, the thermal pressure P, and the electron number density $n_{\rm e}$ at the locations of the tracer particles in the *sSwB* simulation (sSwB = strong Shock, weak B-field; see Sect. 3) for notation . The impact of the shock compression is visible after around 100 Myr. Also the rapid decline of the magnetic field strength due to numerical resistivity is visible. This decline is not observed in 2-d test simulations with either a much higher resolution or a much more ordered magnetic field.

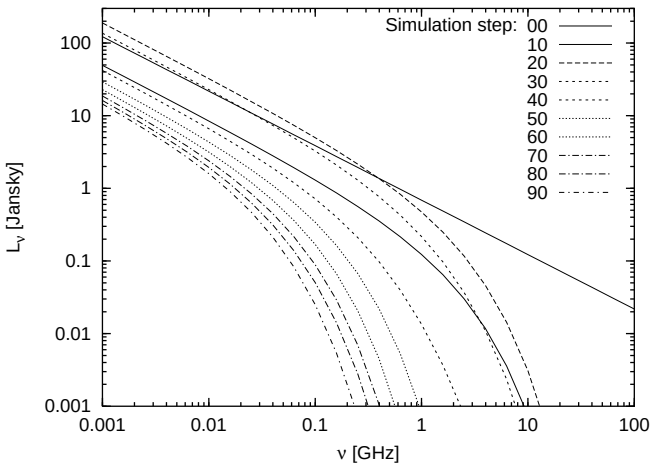

Figure 4. Evolution of the radio spectrum of the *sSwB* simulation. The numbers (00, 10, ..., 90) label different simulation data-dump time-steps. A single time step is approximately 7 Myr long. Clearly visible is the decrease of the cutoff frequency with time. Only in the interval 10-20 (70-140 Myr) the shock compression is able to reverse this. During this phase also the overall emissivity at lower radio frequencies increases mainly due to field strength amplification. At all other time-steps the low frequency flux decreases artificially, due to magnetic field annihilation by numerical field diffusion.

2.2 Radio Maps

The radio maps are constructed using around 10^4 passively advected tracer particles. Initially, each tracer particle is located inside the radio plasma cocoon and is associated with the same initial relativistic electron population. Then the electron spectrum for each tracer particle is evolved in time taking into account synchrotron, inverse Compton, and adiabatic energy losses and gains. In the formalism of Enßlin & Gopal-Krishna (2001)† this spectral evolution requires two quantities to be tracked as a function of time. The first is the compression history, i.e.

$$C(t) = V_0/V(t), \tag{2}$$

where V_0 and $V(t)$ are the initial and present specific volumes of the tracer particles. In our calculations we use the pressure $P(t)$ at the location of the tracer particles to work out the compression via the equation of state:

$$C(t) = (P(t)/P_0)^{1/\gamma_{\rm rp}}, \tag{3}$$

where $\gamma_{\rm rp}$ is the adiabatic index of radio plasma. Even though our MHD simulations have a constant adiabatic index of 5/3, we use $\gamma_{\rm rp} = 4/3$ in Eq. 3 in order to simulate the higher energy gains of the electrons in the more compressible relativistic radio plasma.

The second quantity that has to be tracked in order to evolve the electron spectrum is the energy (or momentum) of an electron that was initially injected with infinite energy. This cutoff momentum p_* of the electron spectrum (here and in the following dimensionless units for electron momenta $p = P_{\rm e}/(m_{\rm e}c)$ are used, where $m_{\rm e}$ is the electron rest-mass, and c the speed of light) is given by

$$\frac{1}{p_*(t)} = a_0 \int_{t_0}^{t} dt' \, (u_B(t') + u_C(t')) \left(\frac{C(t')}{C(t)}\right)^{\frac{1}{3}} . \tag{4}$$

Here $a_0 = \frac{4}{3}\sigma_{\rm T}/(m_{\rm e}\,c)$ with $\sigma_{\rm T}$ the Thomson cross-section, and u_B and u_C are the magnetic and cosmic microwave background energy densities, respectively. Hence the energy evolution of any electron can be calculated using

$$p(p_0, t) = \frac{p_0}{C(t)^{-\frac{1}{3}} + p_0/p_*(t)} . \tag{5}$$

The electron spectrum per dimensionless momentum of a tracer particle $f(p,t)\,dp$ for $p < p_*(t)$ is given by

$$f(p,t) = f_0(p_0(p,t)) \frac{\partial p_0(p,t)}{\partial p} , \tag{6}$$

where

$$p_0(p,t) = p\, C(t)^{-\frac{1}{3}}/(1 - p/p_*(t)) . \tag{7}$$

If the original distribution function is a power-law

$$f_0(p_0) = g_0\, p_0^{-\alpha_{\rm e}} \tag{8}$$

for $p_{\rm min\,0} < p_0 < p_{\rm max\,0}$ the resulting spectrum is

$$f(p,t) = g_0\, C(t)^{\frac{\alpha_{\rm e}-1}{3}}\, p^{-\alpha_{\rm e}}\, (1 - p/p_*(t))^{\alpha_{\rm e}-2} \tag{9}$$

for $p_{\rm min}(t) = p(p_{\rm min\,0}, t) < p < p_{\rm max}(t) = p(p_{\rm max\,0}, t)$.

At fixed intervals during the simulation (up to 100) the positions of the tracer particles as well as the gas and magnetic field properties were written out. These were then used

† Equivalent formalisms were derived and applied to numerical simulations by other authors, e.g. Matthews & Scheuer (1990a,b) , and Churazov et al. (2001) .

to tabulate $C(t)$ and $p_*(t)$ interpolating linearly in the integration in Eq. 4. A second programme read in these tables to calculate the Stokes I-, Q-, and U-polarisation radio maps using the standard integration kernels of synchrotron radiation theory (Rybicki & Lightman 1979). At this step we have specified the parameters of the initial electron spectrum, viewing angle, distance and observing frequency. The maps were stored in the FITS format, and visualised with the radio-astronomical data reduction package AIPS.

3 RESULTS

In the following, results from four simulation runs are presented: two simulations with a weak shock (external compression factor $C_{\rm gas} = 2$), and two with a stronger shock ($C_{\rm gas} = 3.3$). For each shock strength, simulations with dynamically unimportant ('weak') and dynamically important ('strong') field strengths are discussed. In those simulations with strong magnetic fields, the magnetic pressure initially exceeds the thermal pre-shock pressure. But a short violent expansion quickly establishes approximate pressure equilibrium. In the following, we name the simulation with the weak shock and the weak field strength '*wSwB*', with the weak shock and the strong field strength '*wSsB*', and likewise.

Physical units are assumed such that the simulated radio relic resembles one which is located in the denser regions of a small galaxy cluster. In principle, we could assume physical units that correspond to more peripheral relics that reside in lower pressure environments. But in this case the artificially decaying magnetic fields (see Sec. 3.2) have a greater effect on the radio luminosity because the inverse Compton losses are bigger than the synchrotron losses.

The pre-shock external gas density is set to about $5 \cdot 10^{-4}$ electrons/cm^3 and the temperature to 1-2 keV. The simulation box is assumed to have a size of 1 Mpc^3 and to be located at a distance of 100 Mpc from the observer.

3.1 Torus Formation

The passage of a radio cocoon through a shock wave can be seen in Fig. 2. The formation of a torus can be explained as follows: At a shock wave, the ram-pressure of the pre-shock gas (plus its small thermal pressure) and the thermal pressure of the post-shock gas are in balance. But when the lighter radio plasma comes into contact with the shock surface, the ram pressure is reduced at the point of contact. The post-shock gas starts to expand into the volume occupied by the still low pressure radio plasma. This can be seen in the second and third displayed panel of Fig. 2. Finally, the radio plasma is disrupted and a torus forms.

A possible evolutionary scenario of the radio morphology of the cocoon could be similar to what is shown in Fig. 2. In the early stages of the compression the torus has not formed and one expects a sheet like radio relic to be visible. The relic should get more and more edge brightened while the radio plasma accumulates in the torus. Finally, when the thin sheet is disrupted, only a torus-like object should be visible.

Thus we expect that the early, sheet-like radio relics have a 'younger', less steepened spectrum, while the later-stage, filamentary or toroidal relics have a much higher spectral age with a bent, steep radio spectrum.

These predictions are supported by the fact that the relatively sheet-like relics in the cluster Abell 2256 have a flat spectrum (Röttgering et al. 1994) whereas all the filamentary relics in the sample observed by Slee et al. (2001) exhibit steep, bent and therefore 'aged' spectra. We note that this statement needs additional observational confirmation.

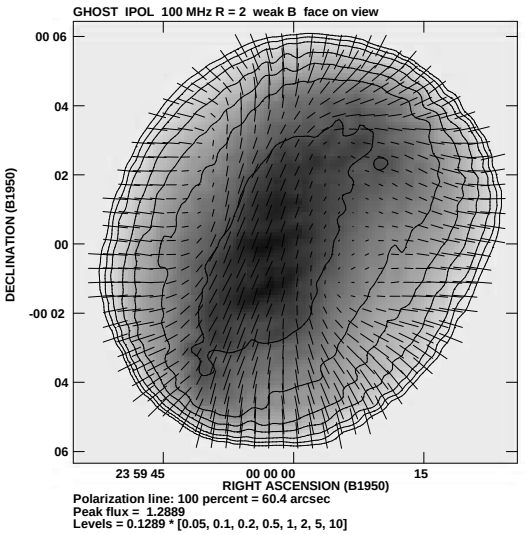

Figure 5. Radio emission of the radio bubble in the model *wSwB* before shock passage. The polarisation E-vectors are displayed by dashes with the length proportional to the relative polarisation. Here and in the following radio maps the flux is given in Jansky per simulation pixel (with linear size of 20.6 arcsec)

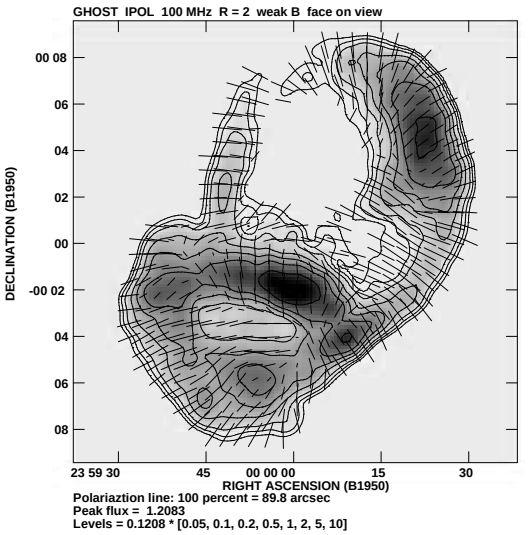

Figure 6. Same as Fig. 5. Late stage of the shock passage in the same model *wSwB*.

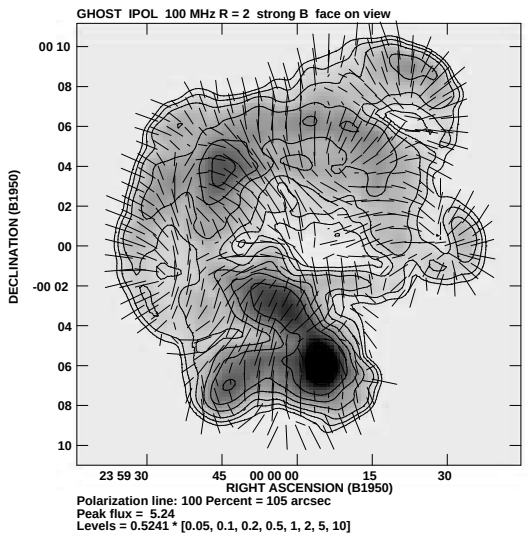

Figure 7. Face-on view of the late stage of the shock passage in the model *wSsB*. For details see Fig. 5.

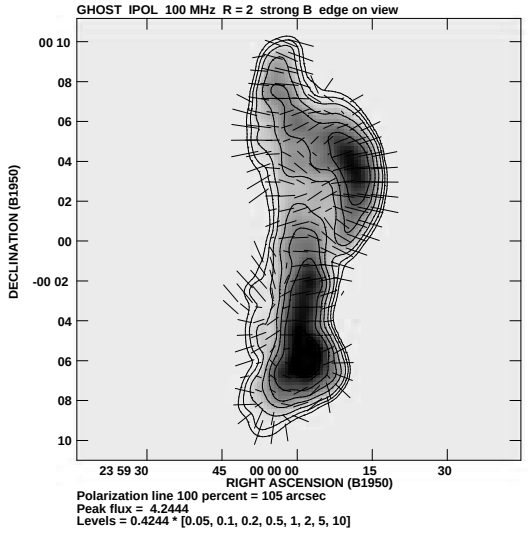

Figure 8. Edge-on view of the late stage of the shock passage in the model *wSsB*. For details see Fig. 5.

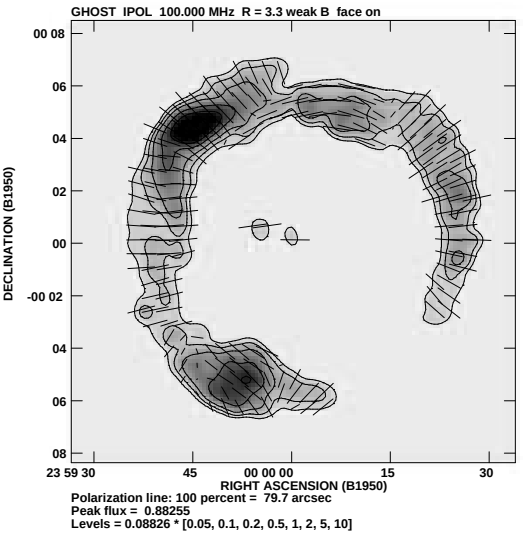

Figure 9. Face-on view of the late stage of the shock passage in the model *sSwB*. For details see Fig. 5.

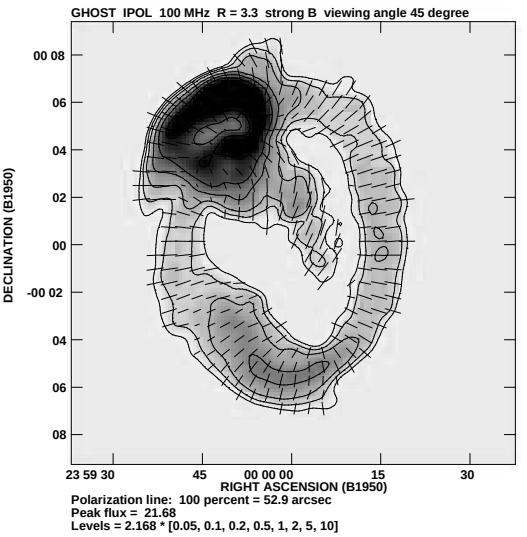

Figure 10. 45 degree view of the late stage of the shock passage in the model *sSsB*. For details see Fig. 5.

3.2 Global Properties

In Fig. 3 the evolution of the average magnetic field strength, the thermal pressure and the electron number density at the location of the tracer particles are shown for one simulation. The bubble reaches its maximal compression after 75-200 Myr. The associated increase in the thermal electron density is somewhat higher than predicted by simple adiabatic compression. This is probably due to gas electrons that have diffused numerically into the radio plasma volume. However, this does not affect our radio maps. The spatial distribution of the relativistic particles is solely determined by the locations of tracer particles. The compressional state of the relativistic electrons is calculated from the fluid pressure and not from the density in order to be less sensitive to numerical diffusion.

Moreover, the decline of the magnetic field strength is caused by the numerical resistivity (or magnetic diffusivity) of the code. The reason for the strong impact of the numerical diffusion of the magnetic field on our results lies in the thin morphology the radio plasma after the shock passage. This brings low density and high density regions, and

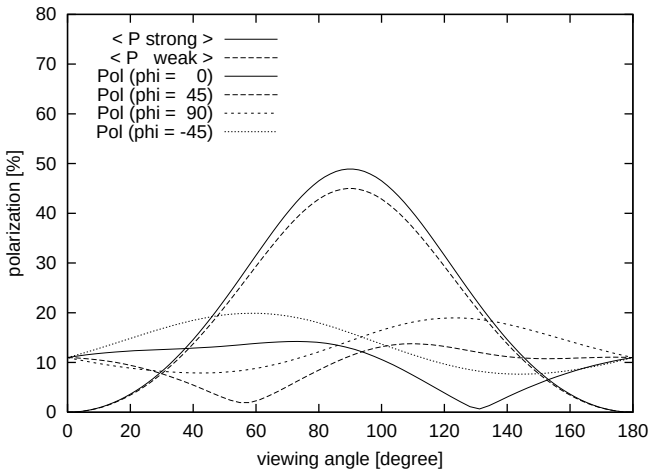

Figure 11. 100 MHz polarisation scans around the radio source in the simulation *wSsB* at an early stage of the shock passage with the viewing angle ranging from face-on (viewing angle = 0°) over edge-on (viewing angle = 90°) to viewing the back (viewing angle = 180°). The different angles $\phi = -45, 0, +45, +90$ label four different routes of the scans around the relic.

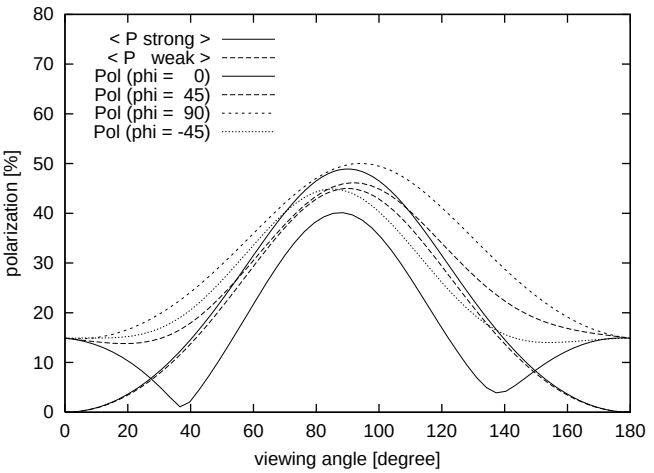

Figure 12. Same as Fig. 11, but for a late stage of the shock passage.

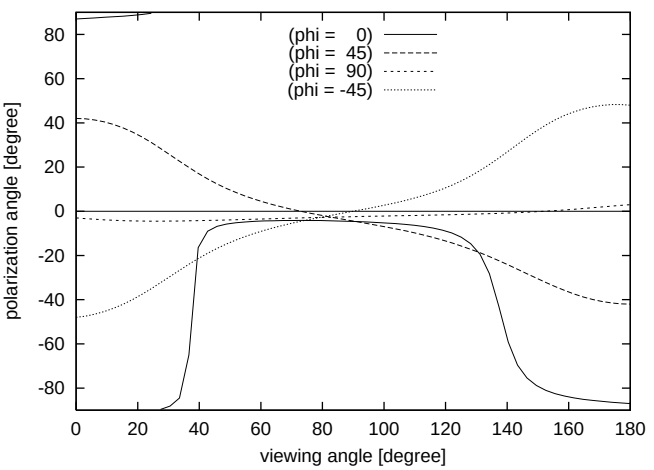

Figure 13. Same as Fig. 12 but here the angle between the projected normal of the shock wave and the E-polarisation vector is displayed. Values near zero mean that the projected magnetic fields are mostly aligned with the projected shock orientation.

also regions with differently oriented magnetic fields close together, producing strong gradients which are sensitive to numerical diffusion. Since the radio plasma is compressed into filaments that are only a few cells wide, magnetic diffusion leads to strong artificial annilihation (or reconnection) of magnetic fields.

Two-dimensional resolution studies indicate that this artificial decrease of the magnetic field strength should become small for a 500^3 cell simulation. Since such a simulation is at present not feasible for us we will try to focus on robust conclusions that are not severely affected by this inaccuracy. However, we have made experiments with low resolution and large-scale fields in two dimensions. These experiments revealed that the magnetic field strength increases drastically upon compression and, subsequently, remains strong – as is expected in the absence of numerical diffusivity.

3.3 Spectral Aging

An increase of a factor ≈ 5 in the radio luminosity during the compression between 70 to 140 Myr can be seen in Fig. 4. However, the greater increase expected from the analytical model of Enßlin & Gopal-Krishna (2001) could not be reproduced in our simulations. This is a result of the decaying magnetic fields due to numerical resistivity, and not a failure of the model. In order not to be too much affected by the rapidly evolving spectral cutoff we restrict our analysis in the following to a low radio frequency, namely 100 MHz.

3.4 Radio Morphology

As the shock wave passes the initially spherical radio cocoon (Fig. 5), the cocoon is torn into a filamentary structure (Figs. 6, 7, 8, 9, and 10). In the simulations with weak magnetic fields the final morphology is toroidal for the strong shock (simulation *sSwB*, Fig. 9) and shows two tori in the case of a weak shock wave (*wSwB*, Fig. 6). Such a double torus seems to be observed in the relic in Abell 85 (Slee et al. 2001, and Fig. 1). The degree of polarisation is relatively high everywhere. The electric polarisation vectors tend to be perpendicular to the radio filaments indicating aligned magnetic field structures within them. The reason for this is that the compression is mostly perpendicular to the filaments since this is how they formed. Therefore, the parallel field component is preferentially enhanced.

But in some few spots (see Fig. 9) the polarisation E-vectors are aligned with the radio filaments. We presume that these spots coincide with regions where the initial magnetic component parallel to the shock was too weak to be amplified above the perpendicular components. Such reversals are indeed observed in polarisation maps of relics but

multi-frequency observations still have to confirm that they are intrinsic, and not induced by foreground Faraday rotation (R. Slee, private communications).

In those simulations where the magnetic fields are dynamically important nearly always a more complicated morphology is produced. In the weak shock simulation (*wSsB*, Figs. 7 and 8) the cocoon does not show any toroidal structure after shock passage. But filamentary structures can still be identified and the E-polarisation vectors seem to be approximately perpendicular to the filaments. The edge-on projection shows that the radio emitting volume is not restricted to the shock plane but also shows kinks and extentions in the flow direction. Similar looking kinks are observed in the radio relics in the cluster Abell 3667. These relics are also likely to be seen edge-on as the merger shock lies within or close to the plane of the sky (Roettiger 1999).

In the simulation with a strong shock and strong fields (*sSsB*) a large torus still appears, but a second smaller one is dominating the total radio emission (Fig. 10). The extreme brightness of this feature is likely to be an artifact of an unlucky realization of the initial random magnetic field configuration than a typical feature of a real radio relic, since a corresponding bright spot already appeared in the initial radio cocoon.

3.5 Radio Polarisation

Our simulations indicate that for a sufficiently turbulent initial magnetic field geometry the total integrated polarisation of a radio relic observed face-on should be small. It is of the order of the total initial fractional polarisation of the source. In the case of a simulated toroidal relic all polarisation orientations are roughly equally present and therefore cancel each other out in the surface integration. But even in a more complex relic, as shown Fig. 7, the integrated polarisation cancels out in the face-on view.

In the edge-on view this is different. Now a preferential direction exists: E-vectors tend to be aligned with the projected shock normal.

It is interesting to study how reliably the overall polarisation strength and direction can be used as a measure of the 3-dimensional shock orientation.

Analytic predictions for the polarisation strength of shock compressed random magnetic fields were already derived in Laing (1980) and Enßlin et al. (1998). In these derivations it was assumed that the compression is linear along the flow axis and that the fields follow completely passively. The resulting percentage radio polarisation is then given by:

$$< P_{\rm weak} >= \frac{s+1}{s+\frac{7}{3}} \; \frac{\sin^2\delta}{\frac{2\,C_{\rm gas}^2}{C_{\rm gas}^2-1} - \sin^2\delta} \; . \qquad (10)$$

The term $C_{\rm gas}$ denotes the shock compression factor, s the spectral index of the electron population, and δ the viewing angle. If the magnetic fields dominate the total pressure one can allow them to expand to pressure equilibrium after shock passage. In this case the polarisation

$$< P_{\rm strong} >= \frac{s+1}{s+\frac{7}{3}} \; \frac{\sin^2\delta}{\frac{2}{15}\,\frac{13 C_{\rm gas}-7}{C_{\rm gas}-1} - \sin^2\delta} \qquad (11)$$

is surprisingly similar to that expected in the weak field case (Enßlin et al. 1998). This can be seen from the reference curves in Fig. 11 and 12.

Also shown in these figures are viewing angle scans of the total polarisation of the radio emission in the simulation *wSsB* before (Fig. 11) and after (Fig. 12) shock passage. These figures show that, in addition to the intrinsic polarisation pattern of the turbulent fields, the shock passage imprints a strong polarisation signature onto the radio plasma.

It is remarkable that the characteristics of the simulated radio polarisation are similar to the analytic models of shocked magnetic fields. If the amplitude of the polarisation curves in our simulations are not too strongly affected by artifacts, such as the decaying field strength, or the incorrect adiabatic index of the radio plasma, we can conclude that the shock acceleration and the revived fossil radio plasma are not distinguishable by this. Alternatively, the simplistic analytic theory of shocked fields seems to be a good guide in relating viewing angle and radio polarisation.

The reason for the similar polarisation pattern in the different models is likely that the magnetic fields in all cases are nearly completely aligned with the shock plane. In the extreme case of completely shock plane aligned fields, but with randomly distributed orientations within that plane, the polarisation is given by

$$< P_{\rm max} >= \frac{s+1}{s+\frac{7}{3}} \; \frac{\sin^2\delta}{2-\sin^2\delta} \, . \qquad (12)$$

This is not too far from the other models.

Whenever the imprinted polarisation dominates over the initial intrinsic one, the direction of the E-vector can be used relatively reliably to infer the shock normal projected onto the plane of the sky (Fig. 13). The angle with respect to this plane can be estimated roughly from the total polarisation.

Thus, in principle, the 3-dimensional orientation (modulo a mirror ambiguity) can be derived from the polarisation data only. However, these points will need additional investigations before it is applicable to real data. Especially the role of the initial field geometry has to be investigated. Our simulated radio ghosts showed deviations from the analytic predictions on the order of the total initial polarisation of the source. Such deviations may significantly reduce the accuracy of any polarisation based viewing angle estimate. However, we think that according to our model there should be a correlation between total polarisation and the viewing angle due to the field ordering action of the shock wave. See Enßlin et al. (1998) for an early attempt to compare these quantities for a small smaple of cluster radio relics.

3.6 Shock Properties

On the basis of our simulations we speculate that the observed dimensions of a cluster radio relic with a toroidal shape may be used to get a rough estimate of the shock strength. This is based on the observation that in the numerical simulations the radius R of the spherical cocoon and the major radius of the torus after the passage of the shock are approximately equal. Since the major (R) and minor (r) radii of the torus can be read off approximately from a sensitive high-resolution radio map, the compression of the radio plasma by the shock can be estimated. In the idealised case

of an initially spherical and finally toroidal radio cocoon, the compression factor is given by

$$C = \frac{V_{\rm sphere}}{V_{\rm torus}} = \frac{4\,\pi\,R^3/3}{2\,\pi^2\,R\,r^2} = \frac{2\,R^2}{3\,\pi r^2}\,. \qquad (13)$$

Assuming the radio cocoon to be in pressure equilibrium with its environment before and after the shock passage, the pressure jump in the shock is given by $P_2/P_1 = C^{\gamma_{\rm rp}}$. If the adiabatic index of the radio plasma $\gamma_{\rm rp}$ is assumed to be known, e.g $\gamma_{\rm rp} = 4/3$ for an ultra-relativistic equation of state, the shock strength can be estimated. But even if this assumption is not justified and the geometry deviates from the idealised geometries assumed here, the strength of the shock wave should be correlated to the ratio of the global diameter of a toroidal relic and the thickness of its filaments. Unfortunately, the quality of the best current radio maps of relics do not yet allow a quantitative comparison of the shock strength by comparing the R/r ratios of toroidal relics. But these maps demonstrate that the necessary sensitivity and resolution might be reached soon.

If, furthermore, the strength of the shock wave of well resolved cluster radio relics can be estimated independently from X-ray maps of the IGM, it would be possible to directly measure the adiabatic index of radio plasma. This can be done by estimating the slope of a $\log(P_2/P_1)$ versus $\log(R/r)$ plot for a sample of well observed radio relics and their shock waves:

$$\log(P_2/P_1) = 2\,\gamma_{\rm rp}\,\log(R/r) - \log(3\,\pi\,\varepsilon/2)\,. \qquad (14)$$

Here ε parametrises the influence of the deviation from the above assumed ideal geometry. The values of ε should scatter from relic to relic, but any systematic correlation of ε with the shock strength should be weak. Even though the present radio and X-ray data do not have the required accuracy yet, at some point in the future this method may enable us to measure the unknown equation of state of radio plasma.

In our simulations the adiabatic index of the simulated fluid ($\gamma_{\rm rp,sim} = \gamma_{\rm gas} = 5/3$) and the shock strength are known ($P_2/P_1 = 3.5$ and $P_2/P_1 = 17.4$ for the shock compression factor $C_{\rm shock} = 2$ and $C_{\rm shock} = 3.3$ respectively). Thus we find that the ratio of the length scales $R/r \approx 3$ for $C_{\rm shock} = 2$ and $R/r \approx 5$ for $C_{\rm shock} = 3.3$. This is roughly consistent with our synthetic radio maps. At least the qualitative correlation of shock strength and diameter ratio is clearly observed, as can be seen in Figs. 6, 9, and 10. Even in the non-toroidal, filamentary case *wSsB* the ratio of the typical filament diameter to the relic diameter seems to be similar to that in the toroidal case, as a comparison of Fig. 7 with Fig. 6 shows.

4 CONCLUSION

We have presented 3-D MHD simulations of a hot, magnetised bubble that traverses a shock wave in a much colder and denser environment. This is assumed to be a fair model for a blob of radio plasma in the IGM which is passed by a cluster merger shock wave. We have calculated radio polarisation maps for the relativistic electron population and computed the spectrum subject to synchrotron-, inverse Compton- and adiabatic energy losses and gains. These maps show that the shock wave produces filamentary radio emitting structures and, in many cases, toroidal structures. Such filaments and tori appear to be observed by very recent high-resolution radio maps of cluster radio relics (Slee et al. 2001). Our simulations find polarisation patterns which indicate that the magnetic fields are mostly aligned with the direction of the filaments. This also seems to be the case for the observed cluster radio relics.

We argued that the formation of filaments and tori is a generic feature of a shock processed hot bubble of plasma whose internal sound speed well above the shock speed. We expect this to be a robust result that will also be found in more realistic simulations, e.g. with the proper equation of state, or more realistic initial magnetic field configurations.

Therefore, we conclude that we have found support for the hypothesis that cluster radio relics indeed consist of fossil radio plasma that has been compressed adiabatically by a shock wave, as proposed by Enßlin & Gopal-Krishna (2001). Thus, the historical name *'cluster radio relic'* seems to be, accidentally or intuitively, an appropriate choice.

From our simulations several predictions about the properties of cluster radio relics can be made – if our scenario is correct :

The formation of the tori and filaments is not instantaneous. First, the simulations show a phase in which the radio plasma is strongly flattened by the shock. During this phase a sheet-like radio relic with a flat spectrum is observed. Later, the radio plasma moves towards the edges of this sheet and finally becomes a torus (or a more complicated, filamentary structure). Since spectral ageing is likely to have affected these later stages, we expect that the filamentary relics have a steeper, more bent radio spectrum than the sheet-like ones.

Our simulations indicate that the diameter D of the bubble of radio plasma remains approximately constant during the passage of the shock. It was also found that the final structure consists of radio filaments of small diameter d that are distributed (often in form of a torus) in an area of diameter D. The compression factor of the radio plasma is proportional to $(D/d)^2$, and this ratio is a measure of the shock strength. Thus, the approximate compression factor of the radio plasma can in principle be read off a sensitive high-resolution radio map. If this number can be estimated for a sufficient number of late-stage relics, and if the pressure jump P_2/P_1 of the shock wave can be obtained from detailed X-ray observations, the unknown adiabatic index $\gamma_{\rm rp}$ of the radio plasma can be computed using the relation:

$$\frac{P_2}{P_1} \propto \left(\frac{D}{d}\right)^{2\gamma_{\rm rp}}\,. \qquad (15)$$

The local radio polarisation reflects the complicated magnetic field structures. But for sufficiently turbulent initial magnetic fields (as in our simulations) the total integrated polarisation of a relic reveals the 3-dimensional orientation of the shock wave. Since the compression aligns the fields with the shock plane, the sky-projected field distribution is aligned with the intersection of the shock plane and the sky plane. Thus, the direction of the total E-polarisation vector yields the sky-projected normal of the shock wave. In principle the angle between the normal of the shock and the plane of the sky can be estimated from the fractional polarisation of the integrated flux. Our simulations indicate

that the viewing angle dependence is similar to that which one would expect if the magnetic fields were embedded in the external gas and passively compressed by a shock, even if this may not be the physical mechanism. But this statement should be treated with some caution since the simulated polarisation may be sensitive to artifacts such as the high numerical magnetic diffusivity and the incorrect adiabatic index of the simulated radio plasma ($\gamma_{\rm rp,sim} = 5/3$ instead of the more likely $\gamma_{\rm rp} = 4/3$). Furthermore, any initial global field orientation may survive the compression and distort this relation between viewing angle and polarisation strength. However, even in this case one expects still a statistical correlation between these quantities. These points need further investigation.

We conclude that this work supports the hypothesis that cluster radio relics are revived bubbles of fossil radio plasma, the so called *radio ghosts*. Spectral aging arguments (Enßlin & Gopal-Krishna 2001) predict the existence of a sizable population of yet undetected cluster radio relics which are only observable with sensitive low frequency radio telescopes.

ACKNOWLEDGEMENTS

We thank O.B. Slee, A.L. Roy, M. Murgia, H. Andernach, M. Ehle for providing us with their observational data prior to publication, and allowing us to display their 1.4 GHz map of the relic in Abell 85. We also thank G. Giovannini and L. Feretti for access to their 330 MHz data of the same relic. We acknowledge A. Kercek's contributions to a very early stage of this simulation project and E. Müller's comments on the manuscript. Some of the computations reported here were performed using the UK Astrophysical Fluids Facility (UKAFF). This work was supported by the European Community Research and Training Network 'The Physics of the Intergalactic Medium'.

REFERENCES

Briel U. G., Henry J. P., 1994, Nature 372, 439,
Burns J. O., Roettiger K., Ledlow M., Klypin A., 1994, ApJL, 427, L87
Churazov E., Brüggen M., Kaiser C. R., Böhringer H., Forman, W., 2001, ApJ, 554, 261
Donnelly R. H., Markevitch M., Forman W., Jones C., David L. P., Churazov E., Gilfanov M., 1998, ApJ, 500, 138
Enßlin T. A., 1999, In Böhringer H., Feretti L., Schücker P. eds., Diffuse Thermal and Relativistic Plasma in Galaxy Clusters. 275, astro-ph/9906212.
Enßlin T. A., Gopal-Krishna, 2001, A&A, 366, 26
Enßlin T. A., Biermann P. L., Klein U., Kohle, S., 1998, A&A, 332, 395
Feretti L., 1999 In IAU Symp. 199, 'The Universe at Low Radio Frequencies'. astro-ph/0006379.
Giovannini G., Feretti L., Stanghellini C., 1991, A&A, 252, 528
Giovannini G., Tordi M., Feretti L., 1999, New Astronomy, 4, 141
Giovannini G., Feretti L., 2000, New Astronomy, 5, 335
Govoni F., Enßlin T. A., Feretti L., Giovannini G., 2001, A&A, 369, 441
Kassim N., Clarke T. E., Enßlin T. A., Cohen A. S., Neumann D., 2001, ApJ, 559, 785
Kempner J. C., Sarazin C. L., 2001, ApJ, 548, 639
Laing R. A., 1980, MNRAS, 193, 439
Miniati F., Ryu D., Kang H., Jones T. W., Cen R., Ostriker J. P., 2000, ApJ, 542, 608
Matthews A. P., Scheuer P. A. G., 1990a, MNRAS, 242, 616
Matthews A. P., Scheuer P. A. G., 1990b, MNRAS, 242, 623
Quilis V., Ibanez J. M. A., Saez D., 1998, ApJ, 502, 518
Roettiger K., Burns J. O., Pinkney J., 1995, ApJ, 453, 634
Roettiger K., Burns J. O., Stone J. M., 1999, ApJ, 518, 603
Roettiger K., Stone J. M., Mushotzky R. F., 1998, ApJ, 493, 62
Röttgering H., Snellen I., Miley G., de Jong J. P., Hanisch R. J., Perley R., 1994, ApJ, 436, 654.
Rybicki G. B., Lightman A. P., 1979, 'Radiative processes in astrophysics'. New York, Wiley-Interscience
Slee O. B., Roy A. L., Murgia M., Andernach H., Ehle M., 2001 AJ, 122, 1172.
Stone J. M., Norman M. L., 1992a,APJS, 80, 753
Stone J. M., Norman M. L., 1992b APJS, 80, 791
Venturi T., Bardelli S., Zambelli G., Morganti R., Hunstead R. W., 1999 In Böhringer H., Feretti L., Schücker P. eds., Diffuse Thermal and Relativistic Plasma in Galaxy Clusters. 27